THE ELECTROCHEMISTRY OF POROUS ZINC IV. THE FARADAIC IMPEDANCE OF PLAIN AND POLYMER-BONDED POROUS ELECTRODES IN KOH SOLUTIONS

N. A. HAMPSON and A. J. S. McNEIL

Department of Chemistry, Loughborough University of Technology, Loughborough, Leicestershire, LE11 3TU (U.K.)

(Received September 24, 1984)

Summary

The electrochemistry of large format porous zinc electrodes (4 cm × 2.5 cm) in 7M KOH solutions has been investigated, using the faradaic impedance technique, as a function of poly(styrene) content and state-of-charge. Both electrode structure and behaviour are complex, but some progress has been made in modelling. Electrodes fabricated on a gauze support conformed to a Randles circuit (charge transfer and solution diffusion) modified to include the effects of product adsorption, electrode roughness, and stray (physical) inductances.

1. Introduction

One approach to the fundamental problem of shape change in secondary zinc electrodes is to incorporate inorganic and/or polymeric additives [1, 2]. Polymeric materials, predominantly polytetrafluoroethylene (PTFE) [3, 4], can be incorporated as a suspension, and subsequent mixing and pressing deforms the polymer so that it binds the electrode structure together (refs. 5 and 6 illustrate this well for PTFE in Pt/C and Pt/Ni electrodes). Another approach, however, is to incorporate the polymer into the zinc electrode using a suitable solvent. This enables a wide variety of polymers to be incorporated, some of which have been found to increase zinc electrode cycle life [7]. We have reported the results of a faradaic impedance study of porous zinc/poly(styrene) microelectrodes elsewhere [8]. Here we report the impedance of large electrodes, as made up for small cell cycling experiments [7], and how this varies with poly(styrene) content and state of charge (SOC). The results of preliminary modelling procedures are also presented.

0378-7753/85/$3.30

2. Experimental procedures

Electrodes were prepared from mercury-free pastes comprising equal proportions of zinc and zinc oxide (both AnalaR grade) and poly(styrene) (code PS1, supplied by RAPRA*, $\bar{M}_N$ = 103 000) dissolved in tetrahydrofuran (AnalaR, 0.1% quinol stabilised) and methanol. Methanol had an important influence on the surface condition of the zinc particles and was essential for the successful fabrication of large format electrodes [7]. Poly(styrene) (PS) was added in solution to make up 2, 10, 20 and 50% of the dry Zn/ZnO mix weight. Electrodes were fabricated by painting on to copper gauze, to reach the weight required for a 1 A h total capacity which, for the PS-free electrode, was 1.35 g of dry paste in a double sided 2.5 × 4 cm format. PS-free electrodes were prepared from both aqueous pastes (Zn(AQ), using M/100 KOH) and non-aqueous pastes (Zn(THF), using THF and methanol). All electrodes were finally prepared by reduction in 7M KOH at 100 mA (*C*/4.4). Electrodes were wrapped in separator material for charging, but impedance measurements were made on bare electrodes, each in a 100 ml beaker containing 90 ml of 7M KOH, with a nickel mesh counter electrode. A full description of the equipment and the experimental procedures has been given elsewhere [7].

All impedance measurements were made on the three-terminal cell, considering the zinc electrode alone, using a frequency response analyser and matching electrochemical interface. The zinc electrode impedances were measured at the rest potential (measured against the Hg/HgO reference electrode) in the fully charged (100% SOC) condition, and in the 90, 75 and 50% SOC conditions. The electrodes were not cycled, but discharged galvanostatically to these charge states at 15 mA (*C*/67 rate).

3. Results and discussion

3.1. The structures of fully charged electrodes

The structures of the fully charged electrodes were examined using a scanning electron microscope (SEM). Specimens were soaked in methanol to remove the KOH, then dried and broken to expose a fracture surface which was coated with 10 nm of sputtered gold. Figure 1 shows a portion of the Zn(THF) electrode interior lying within a grid square of the copper gauze current collector. No structural differences between the Zn(AQ) and Zn(THF) electrodes could be seen. Both electrodes contained very large pores, which were not present in the dried paste and, so, must have been formed during reduction by the parasitic hydrogen evolution reaction. Figure 2 shows the structure of the THF electrode in more detail. The

*Rubber and Plastics Research Association, Shawbury, Shrewsbury, Shropshire SY4 4NR, England.

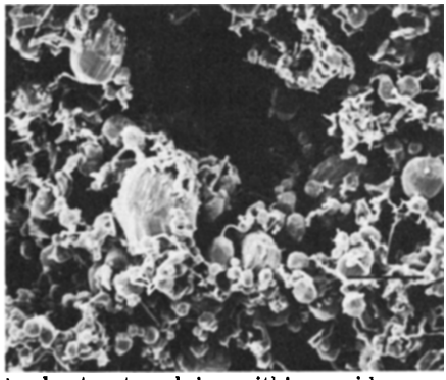

Fig. 1. A general view of the Zn(THF) electrode structure lying within a grid square of the copper gauze current collector (bar = 100 μm).

Fig. 2. The detailed morphology of the Zn(THF) electrode (bar = 10 μm).

structure comprises variously sized grains of zinc, derived from the zinc dust, embedded in a tangle of connected threads which probably derive from the ZnO. The intervening void space is highly convoluted over a considerable size range. This complex structure is the spatial opposite of the transmission line model considered by de Levie [9], in which the electrode material is penetrated by cylindrical, straight pores. Figures 3 - 5 show various aspects of the Zn/PS20 electrode, which illustrate the structural effects of this polymer. The electrode structure is finer and more compacted (Fig. 3), but there is now a disparity between the bulk and superficial conditions. The bulk structure, shown in Fig. 4, is dense; some large pores remain, but generally the scale of porosity is much smaller. The zinc phase tends to be clumps of granules embedded in a ragged continuum of polymer somewhat deformed by the process of fracture. Mass transport would be very limited within this constricted structure, and this condition would be aggra-

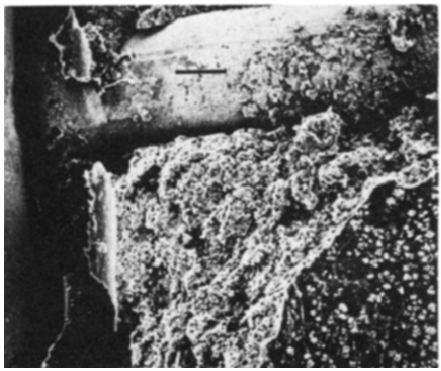

Fig. 3. A general view of the Zn/PS20 electrode, showing the fractured internal structure between the wires of the gauze and the free surface at lower right (bar = 100 μm).

Fig. 4. The internal morphology of Zn/PS20; zinc granules of various sizes embedded in a polymer matrix deformed by fracture (bar = 10 μm).

vated by the polymer skin on the surface (Fig. 5). The active zinc would only be accessible *via* the small holes, through some of which zinc growths have penetrated.

3.2. The Faradaic impedance of fully charged electrodes

Because the zinc electrodes were mercury-free, corrosion in 7M KOH was significant [2, 10]. After charging was completed, with 50% overcharge, the electrodes were allowed to stand for at least 4 h to allow equilibration at the free corrosion potential in the electrolyte before impedance measurements were made.

The spectra of the PS-free electrodes (Zn(AQ) and Zn(THF)) were very similar (see Fig. 6), with a high frequency, inductive tail, one major charge

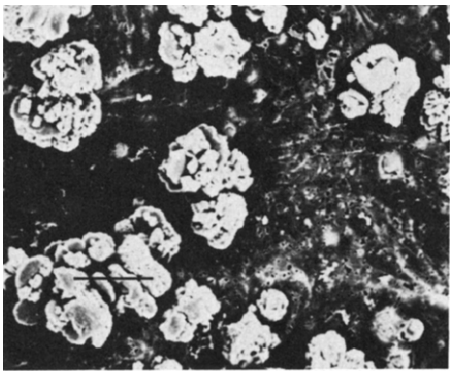

Fig. 5. The surface of the Zn/PS20 electrode; the polymer skin is penetrated by occasional zinc growths (bar = 10 μm).

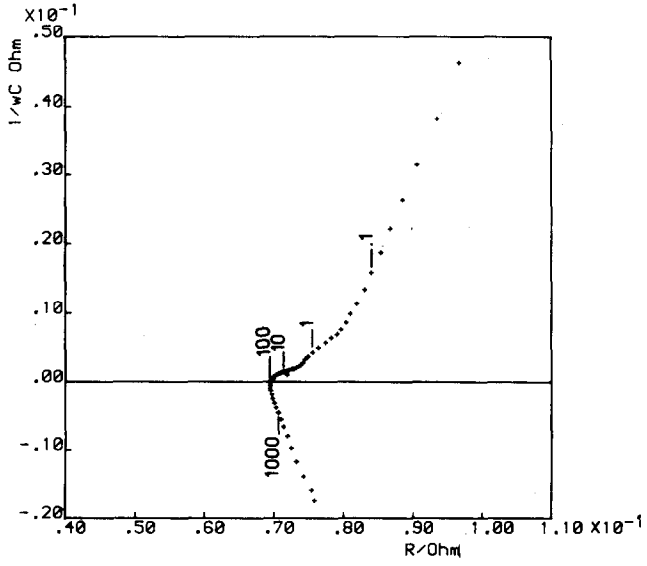

Fig. 6. Impedance spectrum for the Zn(AQ) electrode; SOC = 100%, E_{rest} = −1396 mV.

transfer semicircle with, possibly, a second relaxation process at lower frequencies, and a steep, low frequency locus. There appear to be no significant differences between zinc electrodes prepared by different routes. The impedance locus in Fig. 6 closely resembles the one displayed by porous zinc microelectrodes in 1M perchlorate solutions [8], both in profile, and also in that the scales of features are in the area ratio (0.0707 cm^2 for the microelectrode and $2 \times (2.5 \times 4)$ cm^2 for the large format electrode).

The high frequency inductive tail is a constant feature for all the large format electrodes, whereas it did not appear in the spectra of microelectrodes [8]. Comparative measurements made on another, specially calibrated frequency response analyser proved that this feature originated in the working zinc electrode, and was not an artefact of the instrumentation or the leads. It may be that such inductive behaviour becomes more prominent as electrode dimensions increase, and theoretical considerations [11, 12] have indicated that this feature can arise from the spatial and temporal distribution of electrode processes. Lazarides and Hampson [13] observed an inductive tail in the impedance spectra of porous lead dioxide microelectrodes which was ascribed to the distributed oxygen evolution reaction. It thus seems likely that the inductive feature shown here could originate in the generation of hydrogen within the porous electrode structure. Certainly, this feature could be modelled using a parallel combination of inductance and resistance, as described later.

The impedances of the PS-free electrodes were very low, as shown by the small charge transfer semicircle, and consistent with the very large internal surface area seen in Fig. 2. A second relaxation process could appear (as in Fig. 6), and this is likely to be due to the adsorption of OH-species, which is strong on zinc [14]. At low frequencies the form of the locus was determined by the presence of a surface film formed as a result of the quiescent conditions within the electrode interior. Simple measurements on spectra, such as that in Fig. 6, are of uncertain value because of the distorting effects of porosity and of the high frequency inductive behaviour on the charge transfer semicircle. Nevertheless, the spectrum in Fig. 6 indicates a very low charge transfer resistance (~ 3 mΩ) for the fully charged, plain zinc electrodes, and a very high double layer capacitance of ~ 2 F. This suggests an electrode with a very large accessible internal area. Other measurements on zinc microelectrodes [8] gave a value of ~ 40 μF cm^{-2} for solid electrodes, and an area factor of ~ 70 for porosity in 0.04 cm thick electrodes. From these figures one could expect a double layer capacitance of 0.28 F for large format electrodes ~ 0.2 cm thick. The adsorption of OH^- [14] could push this figure up further.

The incorporation of 2% PS in the zinc electrode produced a large inductive loop in the impedance locus (Fig. 7). Higher levels of addition produced less distinctive discontinuities, which also display a region of decreasing resistance, and at progressively lower frequencies (Figs. 8 and 9). It seems that the presence of PS increased or stabilised the presence of the adsorbed intermediate Zn(I) species which is known to play a part in zinc

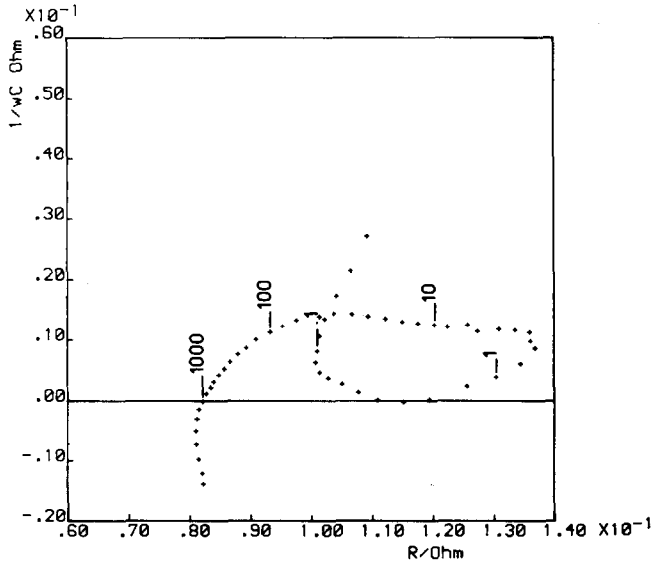

Fig. 7. Impedance spectrum for the Zn/PS2 electrode; SOC = 100%, E_{rest} = −1400 mV.

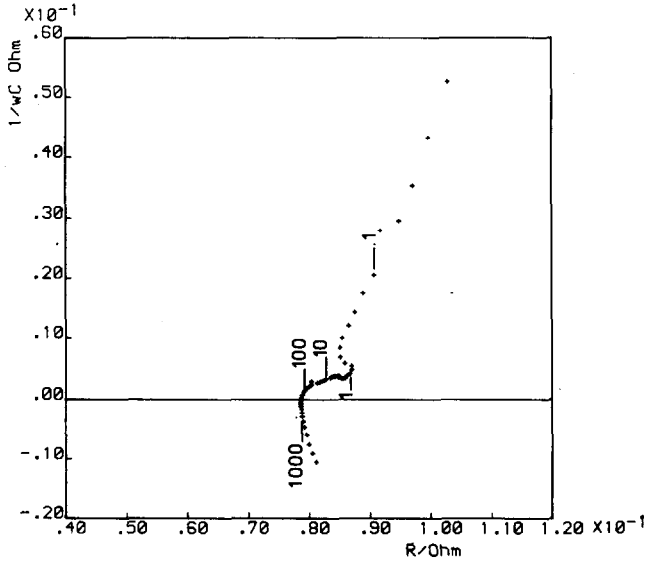

Fig. 8. Impedance spectrum for the Zn/PS10 electrode; SOC = 100%, E_{rest} = −1402 mV.

dissolution in alkaline [15, 16] and other [8] electrolytes, and which is revealed by such loops in the impedance locus [17]. No such feature appears in the spectrum for the PS50 electrode (Fig. 10), possibly because the very low frequencies necessary to reveal it were not attained. The spectrum for this electrode again resembles that for the same electrode in smaller format

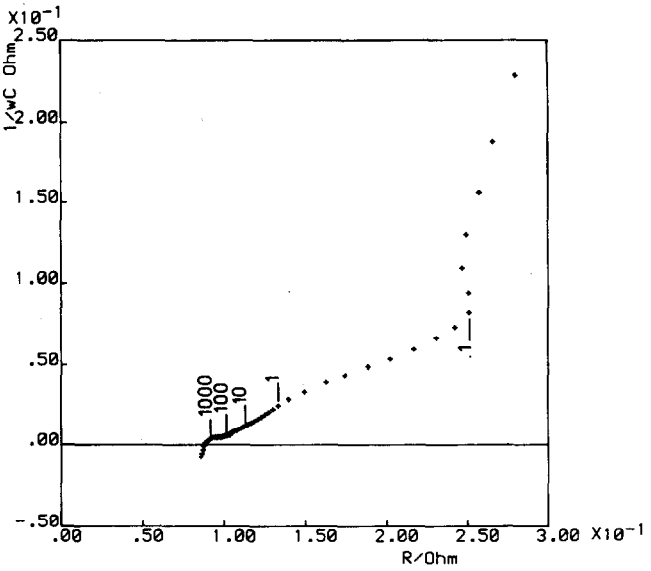

Fig. 9. Impedance spectrum for the Zn/PS20 electrode; SOC = 100%, E_{rest} = −1405 mV.

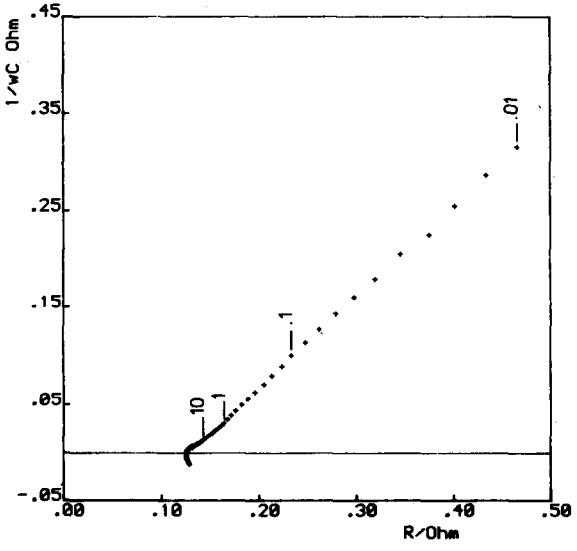

Fig. 10. Impedance spectrum for the Zn/PS50 electrode; SOC = 100%, E_{rest} = −1381 mV.

in perchlorate solutions [8]. That study also revealed that this high level of PS resulted in a much smaller internal area, and this suggests that the large format PS50 electrode would have been less dominated by internal film formation. The electron microscopy suggests that this area reduction is brought about in two ways. First, the zinc takes up a more compact, nodular

morphology, and second, this is to some extent masked by the polymer matrix.

It is hard to assess the degree of porous behaviour of these electrodes in terms of de Levie's predictions [9] for the locus angle, for at both ends of the spectrum, the impedance locus is dominated either by inductive or capacitive influences. The PS20 electrode, however, seems to be highly porous, suggested by the low angle (22°) of the locus between 1 and 0.1 Hz. The PS50 electrode conforms more to solid behaviour.

The incorporation of PS changed the values of charge transfer resistance and double layer capacitance to ~10 mΩ and 0.023 F (PS20), and to 17 mΩ and 0.15 F (PS50). The behaviour suggested by these figures is not clear. If PS were acting solely as a diluent and decreasing the effective surface area of zinc, one would expect changes in charge transfer resistance and double layer capacitance to be in the same ratio. Moreover, the microelectrode study [8] found that the addition of 50% PS diminished electrode activity greatly, to become comparable with that of a solid electrode.

3.3. Partly discharged electrodes

The potential/time discharge profiles for all the electrodes are shown in Figs. 11 - 13, and these are comparable with results reported elsewhere [7]. The plain zinc electrodes suffered little potential drop, even at 50% SOC, and this is reflected in the constancy of impedance spectra at all charge states, which resembled that shown in Fig. 6. Steady discharge at the low rate of 15 mA (*C*/67) would not passivate any part of the electrode, but would decrease the internal area and, hence, the capacitive contribution of the surface film, and this may be the reason for the decreased locus angle at low frequencies. Values of charge transfer resistance and double layer capacitance, however, established from the spectra, changed little with SOC.

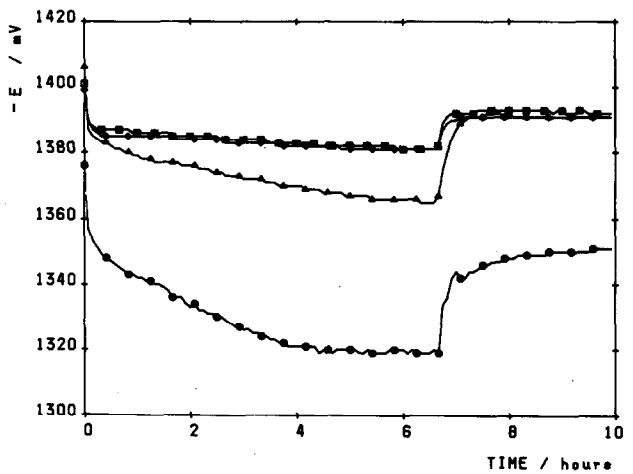

Fig. 11. Potential/time profiles for discharge 100 - 90% SOC: ◇, Zn(AQ), Zn(THF) and Zn/PS2; □, Zn/PS10; △, Zn/PS20; ○, Zn/PS50.

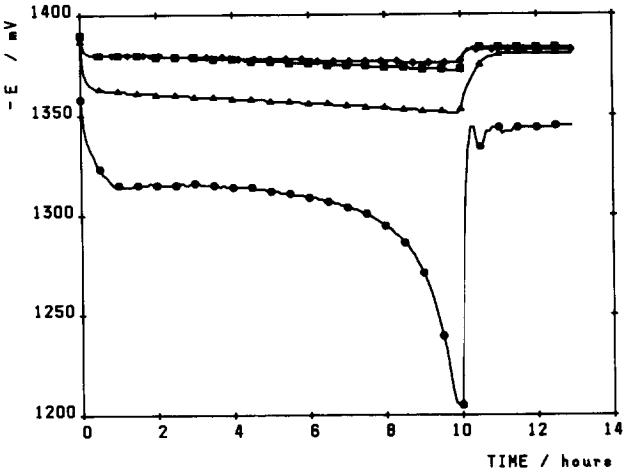

Fig. 12. Potential/time profiles for discharge 90 - 75%; legend as Fig. 6.

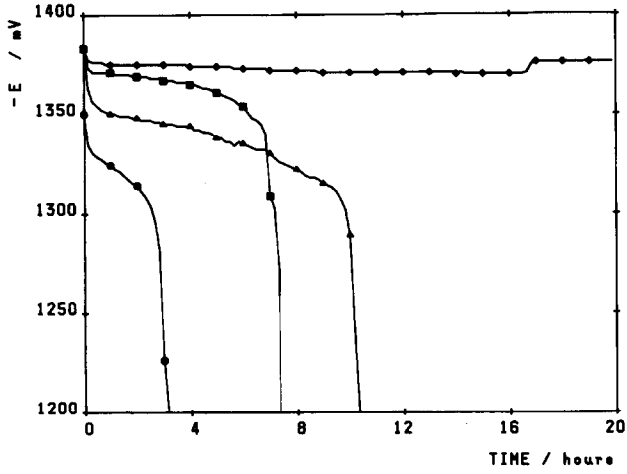

Fig. 13. Potential/time profiles for discharge 75 - 50%; legend as Fig. 6.

By contrast, the partial discharge of the polymeric electrodes had a marked effect on their impedance spectra. The large inductive loop shown by the PS2 electrode at 100% SOC (Fig. 7) shrank, to become a mere break in the continuity of the locus at 90% SOC (Fig. 14). The spectrum for the 50% SOC electrode was similar to that for the PS-free electrode in the same condition (represented by Fig. 6). At higher PS levels, discharge did not significantly change the forms of the loci, but the size of the charge transfer semicircle increased (for example, compare Figs. 15 and 9). As the PS20 electrode was discharged further, the remaining zinc became increasingly inaccessible for current generation. Eventually the electrode failed, clogged by reaction products, the potential dropped precipitously (Fig. 13) and

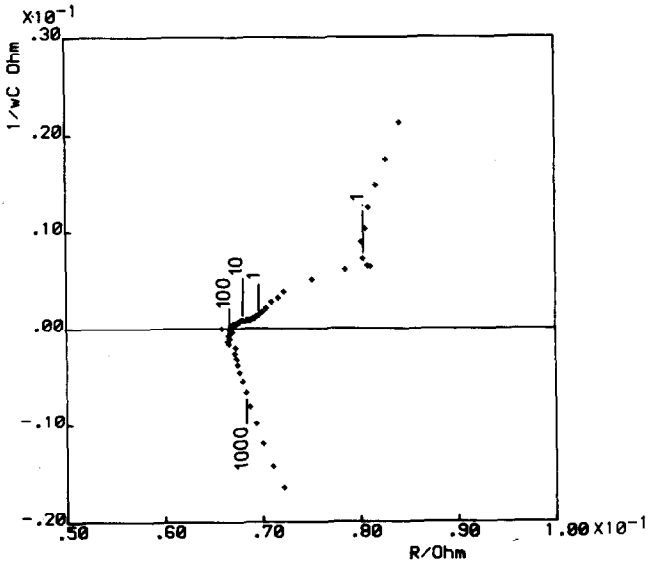

Fig. 14. Impedance spectrum for the Zn/PS2 electrode; SOC = 90%, E_{rest} = −1391 mV.

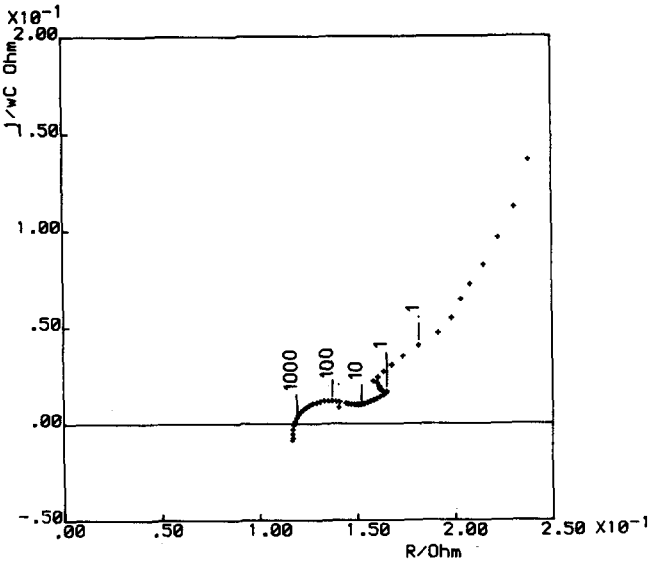

Fig. 15. Impedance spectrum for the Zn/PS20 electrode; SOC = 75%, E_{rest} = −1381 mV.

still had not recovered by the time of the impedance measurement. The impedance spectrum (Fig. 16) became a single, large semicircle, with its centre close to the real axis. The charge transfer resistance, estimated from the diameter, is 64 Ω, comparable with a polymeric zinc microelectrode [8].

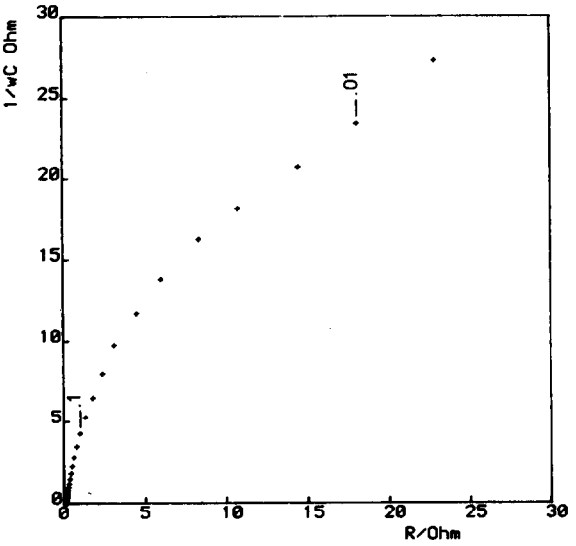

Fig. 16. Impedance spectrum for the Zn/PS20 electrode; SOC = 50%, E_{rest} = −1016 mV.

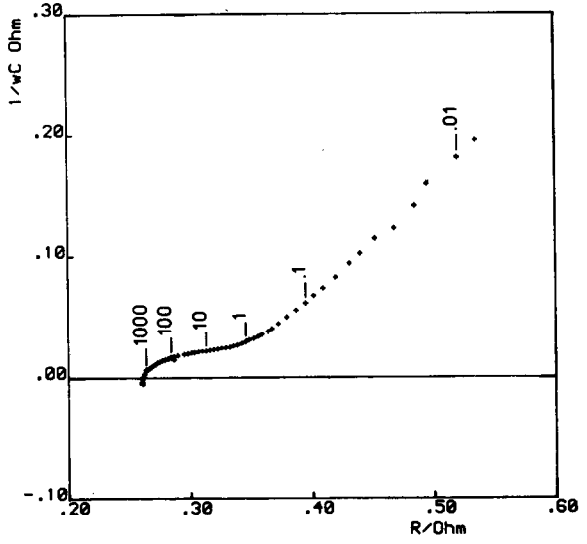

Fig. 17. Impedance spectrum for the Zn/PS50 electrode; SOC = 90%, E_{rest} = −1364 mV.

This suggests that only a small fraction of the zinc remained active, the rest having been "switched off" by the insulating discharge reaction products.

As the PS50 electrode was discharged (Figs. 17 - 19), simple measurements on the spectra suggest the charge transfer resistance to be increased only slightly, but the double layer capacitance to be greatly decreased, from 0.15 F (100% SOC) to 0.025 F (90% SOC) and then to 0.008 F at 75% SOC.

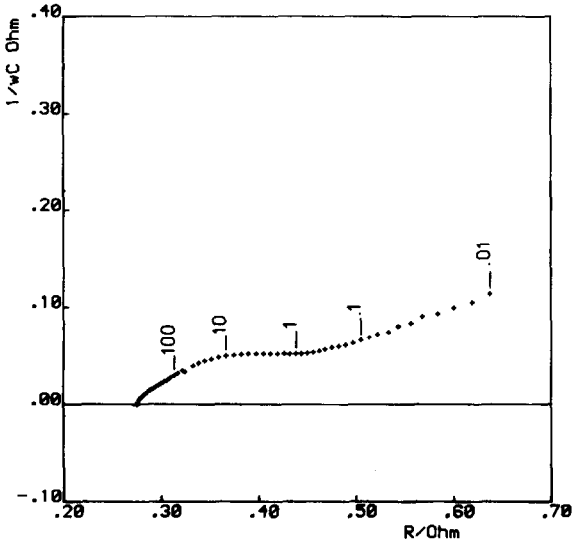

Fig. 18. Impedance spectrum for the Zn/PS50 electrode; SOC = 75%, E_{rest} = −1349 mV.

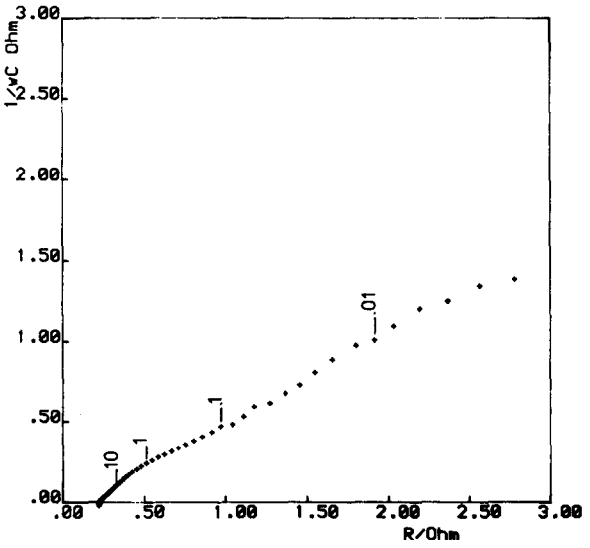

Fig. 19. Impedance spectrum for the Zn/PS50 electrode; SOC = 50%, E_{rest} = −1344 mV.

These conclusions, however, were not supported by the modelling experiments described in the next section. The character of the impedance spectrum also changes in the sequences of Figs. 17 - 19, with the locus lying closer to the real axis, and impedance values increasing, suggesting the electrode to be increasingly clogged by discharge reaction products. All spectra for the PS50 electrode (Figs. 10, 17 - 19) show, in addition to the very small

charge transfer semicircle, a second relaxation semicircle that steadily increases in size until, at 50% SOC, it dominates the charge transfer behaviour.

3.4. Electrode modelling

The impedance spectra discussed above were highly complex, displaying many disparate features. Yet they appear to have a common basis in the Randles equivalent circuit in showing a high frequency charge transfer relaxation process followed by some diffusion in solution. It was felt, however, that the Randles circuit elements could not satisfactorily be determined by simple measurements, because of interference by other features in the spectra. It was therefore decided to attempt to model some of the simpler spectra on an elaborated Randles equivalent circuit, using an iterative procedure on the University mainframe computer [18]. The first form of the circuit tested is shown in Fig. 20, and this could match the spectrum for Zn(AQ) (100% SOC) approximately (Fig. 21), and the spectrum for Zn/PS50 (100% SOC) with more success (Fig. 22). These plots show the fit at

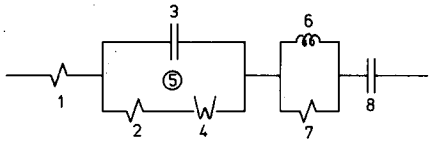

Fig. 20. Elaborated Randles equivalent circuit used to model the impedance spectra of Zn(AQ) and Zn/PS50 both at 100% SOC.

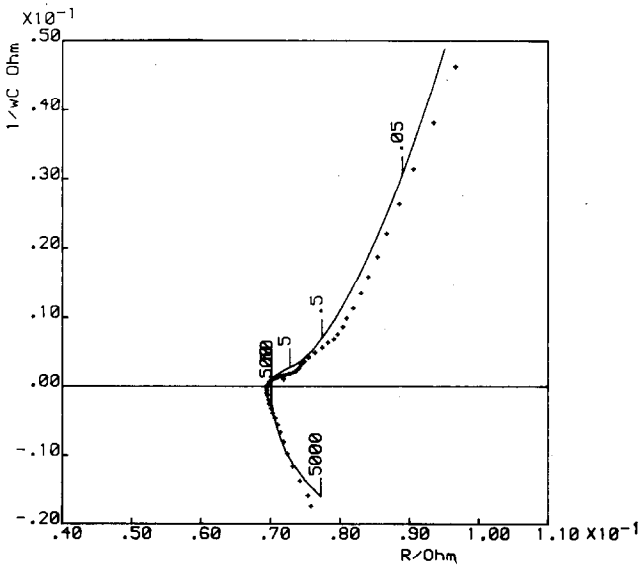

Fig. 21. The calculated spectrum (——) for the circuit in Fig. 20 matched to the behaviour of the Zn(AQ) electrode at 100% SOC. Circuit element values: (1) 0.07 Ω, (2) 0.0032 Ω, (3) 3.83 F, (4) 0.0092 Ω $s^{1/2}$, (5) 1, (6) 6.2×10^{-7} H, (7) 4.3×10^{-2} Ω, (8) 230 F.

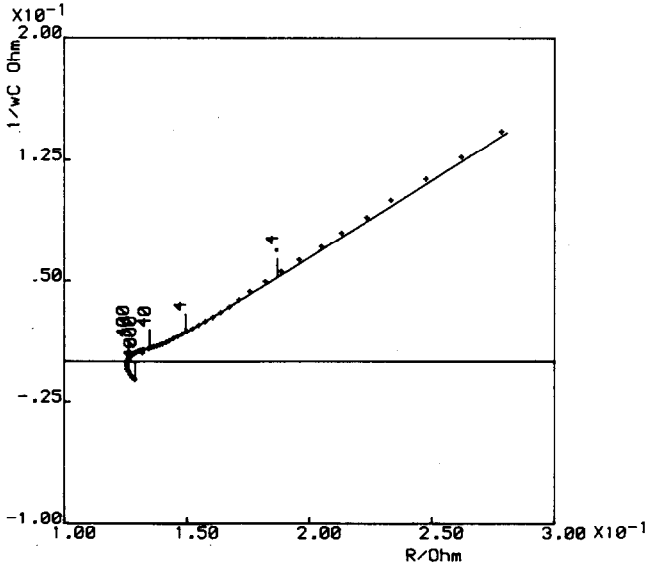

Fig. 22. The calculated spectrum (——) for the circuit in Fig. 20 matched to the behaviour of the Zn/PS50 electrode at 100% SOC. Circuit element values: (1) 0.1248 Ω, (2) 0.0075 Ω, (3) 0.15 F, (4) 0.074 Ω $s^{1/2}$, (5) 0.95, (6) 5.5×10^{-7} H, (7) 4×10^{-2} Ω, (8) 809 F.

the high frequency end of the spectrum; the fit at the low frequency end was good. It turns out that parameter values obtained by simple measurements agree quite well with those obtained by modelling, suggesting that the simpler approach can yield useful results. The model in Fig. 20 incorporated an external, parallel inductance–resistance circuit, and this was able to mimic the high frequency inductive tail observed in the experimental spectra.

As the first model only approximated the behaviour of the Zn(AQ) electrode, which showed a second relaxation process and was inadequate for the discharging PS50 electrode, a second circuit (Fig. 23) incorporating a parallel subcircuit for adsorption was tested. This matched the fully charged Zn/PS50 electrode (shown in Fig. 22) and also the 90% SOC electrode, introducing a second relaxation process (Fig. 24). These values suggest that it was not the double layer capacitance falling with discharge, but the

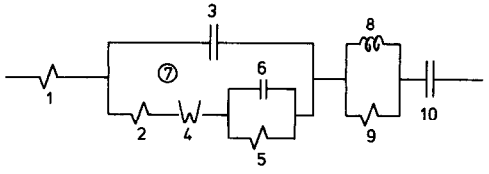

Fig. 23. Elaborated Randles circuit used to model the behaviour of the partly discharged Zn/PS50 electrode.

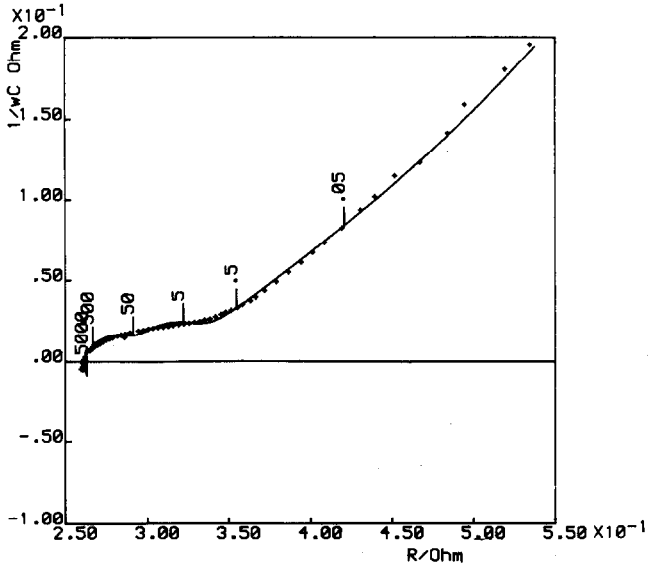

Fig. 24. The calculated spectrum (——) for the circuit in Fig. 23 matched to the behaviour of the Zn/PS50 electrode at 90% SOC. The fit at the low frequency end of the spectrum was good. Circuit element values: (1) 0.258 Ω, (2) 0.008 76 Ω, (3) 0.135 F, (4) 0.0286 Ω $s^{1/2}$, (5) 0.009 78 Ω, (6) 2.24 F, (7) 0.7, (8) 4×10^{-7} H, (9) 4×10^{-2} Ω, (10) 531 F.

roughness factor. This is consistent with an increase in porosity with the removal of zinc from the Zn/PS aggregate, and is in line with changes in the overall shape of the impedance loci. This equivalent circuit, however, was inadequate for modelling the spectra at lower values of SOC.

4. Conclusions

The large format, polymer-bonded, porous zinc electrodes studied in this work are realistic, corresponding to those used commercially, and their structure and behaviour are, accordingly, highly complex. Some progress has been made in characterising and modelling these electrodes, however, both in the fully charged and partly discharged states. While an elaborated Randles circuit (Fig. 15) seems to be an adequate model for these electrodes when they display only one relaxation process, it is inadequate when a second such process becomes significant, and with Zn/PS50 at low charge states.

Acknowledgement

The authors gratefully acknowledge financial support from SERC (for A.J.S.M).

References

1 N. A. Hampson and A. J. S. McNeil, *Electrochemistry*, Specialist Periodical Reports, Royal Soc. Chemistry, Vol. 8, 1983.
2 J. McBreen and E. J. Cairns, *Adv. Electrochem. Electrochem. Eng., 11* (1978) 273.
3 *Brit. Pat. 1,476,550,* 18 March 1975, Electrodes for use in Batteries, Energy Research Corp.
4 J. Goodkin, *Proc. 22nd Annu. Power Sources Conf.*, 1968, p. 79.
5 R. Holze and A. Maas, *J. Appl. Electrochem., 13* (1983) 549.
6 S. Kulcsár, J. Ágh, Á. Fazekas, J. Vigh and Z. Bujdoso, *J. Power Sources, 8* (1982) 55.
7 N. A. Hampson and A. J. S. McNeil, *J. Power Sources,* (1985) in press.
8 P. F. Maher, A. J. S. McNeil and N. A. Hampson, *Electrochim. Acta,* in press.
9 R. de Levie, *Adv. Electrochem. Electrochem. Eng., 6* (1967) 329.
10 L. M. Baugh, F. L. Tye and N. C. White, *Power Sources,* Vol. 9, Academic Press, London, 1983.
11 R. Darby, *J. Electrochem. Soc., 113* (1966) 392; 496.
12 F. Gutmann, *J. Electrochem. Soc., 112* (1965) 94.
13 C. Lazarides and N. A. Hampson, *Surf. Technol., 16* (1982) 255.
14 A. Marshall and N. A. Hampson, *J. Electroanal. Chem. Interfacial Electrochem., 53* (1974) 133.
15 R. D. Armstrong and M. F. Bell, *J. Electroanal. Chem. Interfacial Electrochem., 55* (1974) 201.
16 C. Cachet, U. Ströder and R. Wiart, *Electrochim. Acta, 27* (1982) 903.
17 R. D. Armstrong and M. Henderson, *J. Electroanal. Chem. Interfacial Electrochem., 39* (1972) 81.
18 S. Kelly, N. A. Hampson, S. A. G. R. Karunathilaka and R. Leek, *Surf. Technol., 13* (1981) 349.